THERMAL FLUCTUATIONS OF LARGE CYLINDRICAL PHOSPHOLIPID VESICLES

MARILYN B. SCHNEIDER, JAMES T. JENKINS, AND WATT W. WEBB
Department of Physics, School of Applied and Engineering Physics, and Department of Theoretical and Applied Mechanics, Cornell University, Ithaca, New York 14853

ABSTRACT The time correlation function of the shape fluctuations of large (>10 μm), cylindrical, hydrated, phospholipid-membrane vesicles consisting of one bimolecular layer was measured. The restoring force of the membrane was due to the excess curvature of a membrane element. A value for the curvature elastic modulus, K_C, was obtained from the mean-square amplitude of the normal modes of the fluctuations using the equipartition theorem. An expression for the correlation time was found by solving the dynamics of the membrane's relaxation against the low Reynolds number viscous drag of the surrounding fluid. The amplitudes and correlation times of the fundamental bending mode of the cylindrical vesicles both yield $K_C = 1\text{–}2 \times 10^{-12}$ ergs.

INTRODUCTION

Phospholipid vesicles whose walls consist of a single bilayer are currently of interest as models of cell membranes (1–4), as systems of two-dimensional intermolecular ordering (5–8), and for their material properties (9–15). The equilibrium shape of a flaccid vesicle, for a given area and volume, is determined by the minimization of the elastic energy due to the curvature of a membrane element (11,16). These calculations have also shown that the shape of the red blood cell can be explained by considering only the curvature energy of its membrane (11,16). We suggest that, for small deformations of long wavelength, the dominant mechanical parameter of the membrane in flaccid eucaryotic cells is also the curvature elastic modulus.

Theoretically, the magnitude of the phospholipid membrane's curvature elastic modulus could be deduced by measuring the shape of the vesicle as a function of the hydrostatic pressure excess of the water exterior to the vesicle over that interior to the vesicle. Because the curvature modulus is very small (12,17), the required pressure excess is only $\sim 10^{-3}$ dyn/cm^2, which is too small to measure. However, the smallness of the curvature modulus means that there are many thermally accessible shapes having the same area and volume that are within k_bT of the equilibrium configuration of the flaccid vesicle. For this reason, the shapes of thin-walled vesicles are observed to fluctuate (5,12); this is believed to be the same phenomenon as the so-called "flicker" of red blood cells (17-19).

Measurements of these thermal excitations have been used to deduce a value for the curvature elastic modulus, K_C, of red blood cells and artificial vesicles. Brochard and Lennon (17) measured the frequency spectrum of the fluctuations of the central thickness (a peristaltic mode) of the red blood cell and found $K_C \sim 3 \times 10^{-13}$ ergs. Servuss et al. measured the mean-square amplitude of the bends of long unilamellar cylindrical vesicles and found $K_C \sim 2 \times 10^{-12}$ ergs (12). Surprisingly, the artificial vesicles appear to have a larger curvature elastic modulus despite the fact that the membrane of the red blood cell consists of lipids similar to those in the artificial membrane with the addition of cholesterol, integral proteins, and a polymeric protein cortex. Because some of the integral proteins are attached to the spectrin-actin polymeric network (20, 21) beneath the cell membrane, this structure is expected to affect the behavior of the red cell membrane. The experiments of Evans and co-workers show the importance of the cytoskeleton network in resisting shear deformations and large-scale area changes (22, 23). However, the network might be expected to stiffen the membrane, not to decrease K_C. This discrepancy between the experiments on red blood cells and on artificial vesicles motivated this work.

The red blood cell experiments measured the dynamics of a peristaltic mode and were analyzed using a planar membrane approximation. The artificial membrane experiment measured the amplitude of a bending mode. In the present work, we extend the second study to include the dynamics of the fluctuations by measuring the time correlation function of the fundamental bending mode in tubular vesicles. We use a linear response theory to deduce values for the curvature elastic modulus from both the amplitudes and the spectra of the fluctuations.

The form of the curvature elastic energy of a vesicle is (9,10)

$$E_{tot} = \frac{1}{2} K_C \iint \left(\frac{1}{R_1} + \frac{1}{R_2}\right)^2 dA \qquad (1)$$

where dA is an area element of the membrane and R_1 and R_2 are the two principal radii of curvature (24). Eq. 1 assumes that the two sides of the membrane bilayer are identical. If this were not true, the membrane might

spontaneously curve; this can be taken into account by subtracting a constant from the curvature sum before squaring (10,11).

The fluctuations are treated by supposing that the only important contribution to the excess energy of a thermally fluctuating vesicle is from the curvature elastic energy (5,12). When the shape of the fluctuating vesicle can be expanded in a set of normal modes that are linearly independent of the functions describing the equilibrium shape, the equipartition theorem gives the average excess curvature energy per mode as $k_bT/2$. The expression for the curvature energy of each mode is roughly $K_C\, Q^4\, \langle U^2 \rangle\, A$ (25), where U and Q are, respectively, the amplitude and wave number of a mode, and A is the area of a vesicle. The brackets denote an ensemble (or time) average. A measurement of the mean-square amplitude of a mode, $\langle U^2 \rangle$, will yield a value for K_C. Each of the independent modes contributing to the description of the shape of the vesicle possesses a characteristic correlation time, τ_C. The time correlation function (26) of a mode is

$$\langle U(\tau)U(0) \rangle = \langle U^2 \rangle\, e^{-\tau/\tau_C}. \tag{2}$$

An expression for the correlation time of a mode is obtained by solving the dynamical problem of the vesicle excited into a normal mode and relaxing back to its equilibrium shape. In this process, the restoring force of the membrane's curvature elasticity is balanced by the viscous resistance of the surrounding fluid. The membrane fluid is also viscous, but for long wavelength fluctuations its resistance to shearing is negligible (14, 15) compared with that of the surrounding fluid. The restoring force is given by the negative of the functional derivative of the curvature energy with respect to the fluctuation amplitude U:

$$F = -\frac{\delta E}{\delta U}. \tag{3}$$

The motion of the surrounding fluid is described by the linearized Navier-Stokes equations and the continuity equation. The small size of the vesicles (~10 μm) and the long relaxation times (~1 s) allow the inertia of the fluid to be neglected. The problem falls then into the regime of low Reynolds number hydrodynamics (27). The velocity of the fluid at the membrane is equated to the membrane velocity, the elastic restoring force is balanced by the viscous drag of the fluid, and the resulting expressions solved for τ_C as a function of K_C.

The amplitude and the correlation time of a bending mode in long cylindrical vesicles was measured. We found $K_C \sim 1\text{–}2 \times 10^{-12}$ ergs, in agreement with Servuss et al. (12). The approximations made in our theory for the long tubes were too crude for us to apply the theory to measure K_C from the peristaltic fluctuations.

In another paper, we report theoretical and experimental (Schneider, M. B., J. T. Jenkins, and W. W. Webb, manuscript in preparation) measurements on quasi-spherical vesicles. We again find $K_C \sim 1\text{–}2 \times 10^{-12}$ ergs.

THEORY

We consider here the dynamics of the bending modes of long cylindrical vesicles. With L the tube length and a the tube radius, we treat tubes for which $L >> a$. We measured the time correlation function of the displacement $u(t)$ of the mid-section of the tube from the midpoint of the line connecting the two ends of the tube (Fig. 1).

To find an expression for the time correlation function, $\langle u(\tau)u(0) \rangle$, we calculate two extremes, the fluctuations of a long string ($u \geq a$) and the fluctuations of a long sausage ($a >> u$). The calculations for $u \geq a$ and $a >> u$ give identical expressions for the amplitude of the fluctuations and differ by a factor of 2 in their correlation times. The observations reported are for cylinders with $\langle u^2 \rangle \sim a^2$.

$L >> u \geq a$

This is the limit that Servuss et al. (12) considered. We first calculate the curvature energy (Eq. 1) of a curved tube and express it in terms of a set of normal modes. To find R_1 and R_2, the principal radii of curvature in Eq. 1, we consider a bend in the cylinder such that the cylinder remains in a plane (Fig. 2 *a*) and the cross section remains circular. Taking R as the radius of curvature of the axis of the cylinder and defining the outward normal as positive, it can be seen from Fig. 2 *b* that $R_1 = -a$ and $R_2 = -(a\cos\xi + R)/\cos\xi$. Also, from Fig. 2 *a*, $dA = aR_2\cos(\pi - \xi)d\xi d\omega$ and $dz = R\, d\omega$. Consequently, the free energy of the bent cylinder is

$$E_{tot} = \frac{1}{2} K_C \int_{-L/2}^{L/2} \int_{-\pi}^{\pi} \left[\frac{-1}{a} - \frac{\cos\xi}{R + a\cos\xi} \right]^2 \cdot (R + a\cos\xi)\, \frac{a}{R}\, d\xi\, dz. \tag{4}$$

We consider only those cylinders for which $|R| \geq L$. Then, upon using $L >> a$ and $|R| >> a$, expanding in powers of a/R, keeping the quadratic terms, integrating over ξ, and subtracting $\pi K_C L/a$ (the curvature energy of the straight cylinder), the free energy due to bending is

$$E = \frac{a\, K_C\, \pi}{2} \int_{-L/2}^{L/2} \frac{dz}{R^2}. \tag{5}$$

This is Eq. 5 in Servuss et al.(12).

Suppose the cylinder always remains in the xz plane and its equilibrium position is along the z axis between $-L/2$ and $L/2$. The x coordinate of the position of the cylindrical axis, $w(z,t)$, may be expanded in a

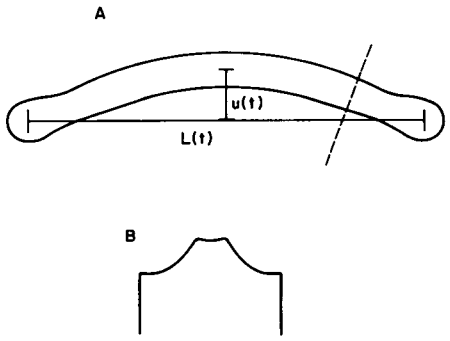

FIGURE 1 Sketch of a measurement on a cylindrical vesicle. (The fluctuation amplitude is exaggerated for clarity.) (*A*) The measured quantities $u(t)$ and $L(t)$ are defined as shown. The dotted line in *A* is the path used for the fluorescence intensity vs. distance sketch in *B*.

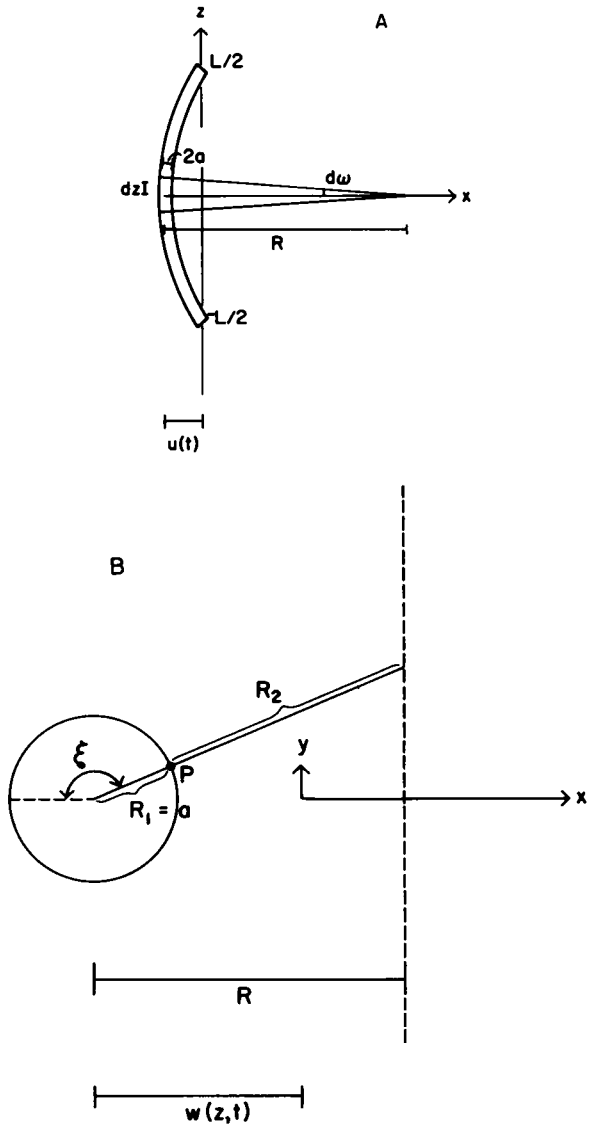

FIGURE 2 Notation used in the calculations for the fluctuations of a cylindrical vesicle for case 1 ($u \geq a$). (A) The xz plane. The experimentally measured quantity is $u(t) = w(0,t) - w(L/2,t)$. (B) The xy plane for $(-L/2) \leq z \leq (L/2)$. R_1 and R_2 are the principal radii of curvature.

Fourier series in z. If the length along the z axis of an element of cylinder is unchanged (to first order) during the bending, then $R = \partial^2 w/\partial z^2$. Because we did not observe distortions at the end points of the vesicles, we concluded that the hemispherical ends remain unstressed during the fluctuations and, therefore, the appropriate boundary condition is that the curvature at the end points is zero. (Note that on the average the cylinder does not translate or rotate.) Then

$$w(z, t) = \sum_{m=0}^{\infty} W_m \cos(\pi m z/L), \tag{6}$$

where $W_m = W_m(t)$. In this normal mode expansion, the $m = 0$ term describes the displacement of the end points of the cylinder. The curvature energy may be expressed as

$$E = \frac{a K_C \pi}{2} \int_{-L/2}^{L/2} \left[\frac{\partial^2 w}{\partial z^2}\right]^2 dz = \frac{a K_C \pi L}{4} \sum_{m=1}^{\infty} \left[\frac{\pi m}{L}\right]^4 W_m^2. \tag{7}$$

The time correlation function $\langle w(z,\tau)w(z,0)\rangle$ can be expressed as a sum of the time correlation functions of the linearly independent Fourier amplitudes, $\langle W_m(\tau)W_m(0)\rangle$. The expression for the time correlation function is determined from Eq. 6 and Eq. 2 with $U = W_m \cos(\pi m z/L)$ as

$$\langle W(z, \tau)W(z, 0)\rangle = \sum_{m=1}^{\infty} \langle W_m^2\rangle \cos\left(\frac{\pi m z}{L}\right) e^{-\tau/\tau_m}, \tag{8}$$

where τ_m is the correlation time of the mth mode. Setting the energy per mode equal to $k_b T/2$ in Eq. 7, we obtain the contribution to the correlation function amplitude per mode as

$$\frac{\langle W_m^2\rangle}{L^2} = \frac{2 k_b T}{K_C \pi^5 m^4} \frac{L}{a}. \tag{9}$$

To find the correlation time, we calculated the velocities of the membrane and the fluid, the restoring force of the membrane, and the drag force of the fluid as the vesicle relaxes back into its equilibrium shape from its excited state, described by Eq. 6.

The elastic restoring force per unit length is given by the negative of the functional derivative of the free energy (Eqs. 3,6,7):

$$F = -a K_C \pi \frac{\partial^4 w}{\partial z^4} = -a K_C \pi \sum_{m=0}^{\infty} \left[\frac{m\pi}{L}\right]^4 W_m \cos\frac{\pi m z}{L}. \tag{10}$$

The viscous drag is calculated in the low Reynolds number limit by placing two series of point velocity sources along but normal to the axis of the cylinder in such a way that the Stokeslet source, which decays like the inverse of the distance, is proportional to and in the direction of the elastic restoring force at that point. The dipole source decays like the inverse of the distance cubed and does not generate a pressure field, so there is no restoring force associated with it. The strength of the dipole source is chosen so that the boundary conditions on the fluid velocity are satisfied on the surface of the cylinder (Fig. 3) (28,29).

For an infinitely long circular cylinder, the slow decay of the Stokeslet sources leads to the Stokes paradox. That is, there is no solution to the creeping-motion limit of the Navier-Stokes equations that satisfies the boundary conditions on the velocity both at the surface of the cylinder and at infinity. However, if the cylinder has a finite length, the velocity field will decay inversely with distance at distances on the order of the length of the cylinder and longer (27–29).

Lighthill (29) has calculated the viscous drag for a finite straight cylinder moving normal to its axis with a velocity V. He finds that the

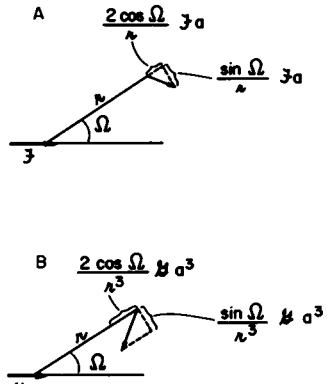

FIGURE 3 (A) Stokeslet velocity source showing slow decay of the velocity field. (B) Dipole velocity source. The velocity fields are rotationally symmetric around the axis of the velocity sources. The velocity sources, $\mathcal{F}$ and $\mathcal{G}$, are placed along but perpendicular to the axis of the cylindrical vesicle.

viscous force per unit length, F_{norm}, acting at the point on the axis a distance c from one end of the cylinder and b from the other end is

$$F_{norm} = \frac{-8\pi\eta V}{1 + \ln(4cb/a^2)}. \quad (11)$$

If the axis of the cylinder is curved with wavelength λ, then the point sources are linearly aligned only for a distance of roughly 0.09 λ. In this case, Lighthill (29) replaces cb in Eq. 11 with $(0.09\ \lambda)^2$. We emphasize that this is valid only if the amplitude of the undulation, while small compared with the wavelength, is not small compared with the radius of the cylinder, because the correction to the velocity field at the surface of the cylinder is on the order of w/a.

Using $V = \partial w/\partial t = \Sigma[\partial W_m(t)]/\partial t \cos(\pi\ mz/L)$ in Eq. 11, and equating Eq. 11 to Eq. 10, we find $W_m(t) = W_m e^{-t/\tau_m}$ where

$$\tau_m = \frac{4\eta}{K_C}\left[\frac{L}{\pi m}\right]^3 \frac{1}{\pi\{\ln[L/(am)] - 0.52\}} \frac{L}{am}, \quad (12)$$

and we have set $cb = (0.09\ 2L/m)^2$.

We measured the time correlation function, $\langle u(t)u(0)\rangle$, of the displacement of the midsection of the tube from the midpoint of the line connecting the two ends, where $u(t) = w(0,t) - w(L/2,t)$. The measured correlation function is thus given by Eq. 8 with $z = 0$. Because both $\langle W_m^2\rangle$ given by Eq. 9 and τ_m given by Eq. 12 are proportional to $1/m^4$, the $m = 1$ term dominates, yielding

$$\frac{\langle u(\tau)u(0)\rangle}{L^2} = \frac{2k_bT}{K_C\pi^5}\frac{L}{a}e^{-\tau/\tau_1}, \quad (13a)$$

and

$$\tau_1 = \frac{4\eta}{K_C}\left[\frac{L}{\pi}\right]^3 \frac{1}{\pi\ [\ln(L/a) - 0.52]}(L/a). \quad (13b)$$

$$L >> a >> u$$

In this limit, we first consider the general case of small fluctuations of a "sausage-like" vesicle. The types of fluctuations include pure bending modes (the cross-sectional area of a piece of tube perpendicular to the tube's axis remains constant as the position of the axis fluctuates), pure peristaltic modes (the cross-sectional area is increased or decreased but the axis of the cylinder remains stationary), and mixed modes. We adopt a cylindrical polar coordinate system with ρ, ψ, and z, respectively, the radial, circumferential, and longitudinal coordinates. The axis of the undeformed vesicle is along the z axis, and it is assumed that the axis remain in the xz plane (Fig. 4). We first allow only deformations, $s(\psi,z,t)$, in the radial direction. The fluctuating shapes can be expanded in the series

$$s(\psi, z, t) = \sum_q \sum_{k=0}^{\infty} S_{qk}(t) \begin{matrix}(\sin qz)\ (\cos k\psi)\\ (\cos qz)\ (\sin k\psi)\end{matrix}. \quad (14)$$

To find the curvature energy (Eq. 1) of the fluctuating vesicle in Fig. 4, notice that $1/R_1 = (-1 + \partial^2 s/\partial\psi^2)/\rho$. But $\rho = a + s$, so $1/R_1 = (-1/a) + (s/a^2) + \partial^2 s/\partial\psi^2$ and $1/R_2 = \partial^2 s/\partial z^2$, where the outward normal is again taken as positive. The membrane's compressibility is negligible, so the area element remains constant and the curvature elastic energy of the bent cylinder above that of the straight equilibrium cylinder is

$$E = (1/2)\ K_C \int_{-L/2}^{L/2}\int_0^{2\pi}\left(\frac{s}{a^2} + \nabla^2 s\right)^2 a\ d\psi\ dz. \quad (15)$$

Using the expression in Eq. 14, this may be written as

$$E = \sum_q \sum_{k=0}^{\infty} \frac{1}{4} K_C \frac{a}{L}\left(\frac{1-k^2}{a^2} - q^2\right)^2 \frac{S_{qk}^2}{L^2}. \quad (16)$$

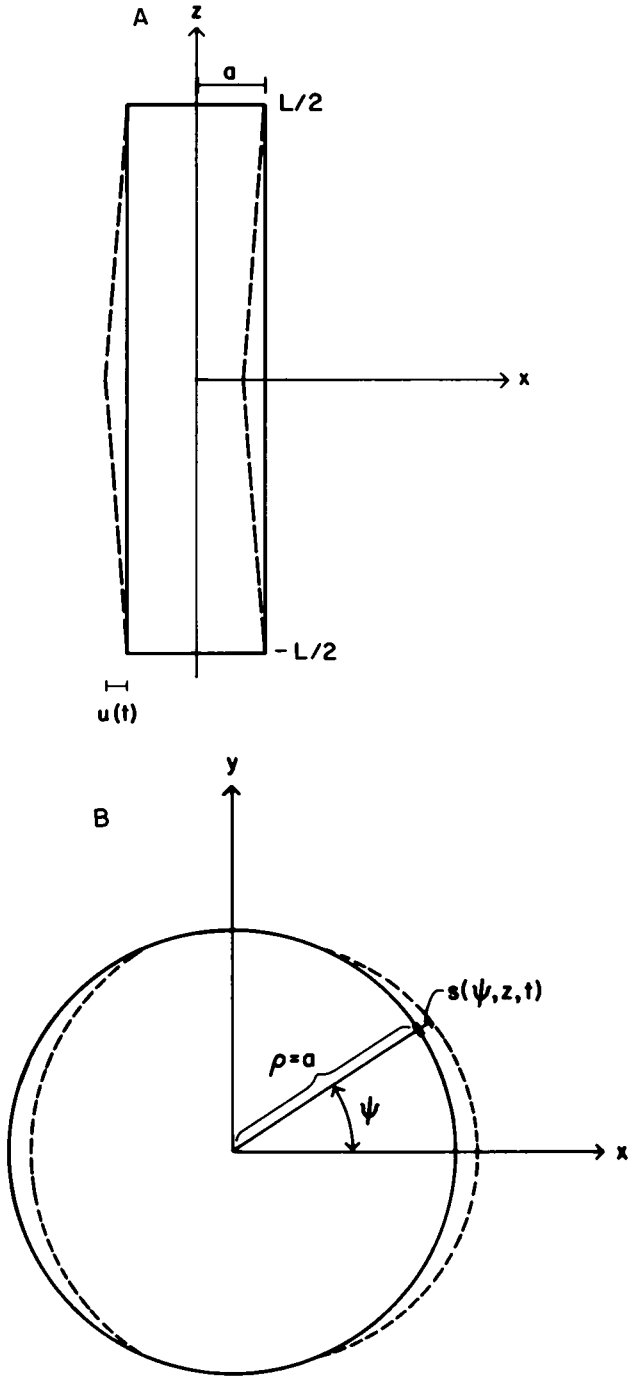

FIGURE 4 Notation used in the calculations for the fluctuations of a cylindrical vesicle for the case where ($u << a$). (A) The xz plane. The experimentally measured quantity is $u(t) = s(0,0,t) - s(0,L/2,t)$. ($B$) The xy plane for $(-L/2) \leq z \leq (L/2)$. The fluctuation in the radial direction is $s(\psi,z,t)$.

Finally, upon taking the ensemble average and setting the average energy in each mode equal to $k_bT/2$, we obtain

$$\frac{\langle S_{qk}^2\rangle}{L^2} = \frac{2k_bT}{K_C\pi}\frac{L}{a}\frac{1}{[(1-k^2)/a^2 - q^2]^2}. \quad (17)$$

For the pure peristaltic mode ($k = 0$), q must be in integral multiples of $2\pi/L$ to conserve volume. The instabilities in this mode, occurring for

values of $L/a = 2\pi m$, where m is an integer, correspond to the breakup of a long fluid cylinder into spherical drops (30). A result of this instability is the "strings of pearls" often observed both in preparations of lipid vesicles (31, 32) and in tethers of the red cell membrane at temperatures above 51°C (33) (the thermal transition temperature of the spectrin). The predicted amplitudes of the pure peristaltic fluctuations of a stable cylinder are very sensitive to the proximity of L/a to multiples of 2π. Because L/a could not be accurately determined for the cylindrical vesicles we observed, our theory cannot be used to obtain a value for the curvature elastic modulus from measurements of this mode.

The pure bending modes have $k = 1$. Again, the ends of the cylinder remain unstressed, so these modes have zero curvature at the ends. Only the cosine terms with q, an integral multiple of π/L, appear in Eq. 14. The appropriate expression for the apparent amplitude of the bend of the cylindrical axis in the plane at $z = 0$ (Fig. 4) will involve only odd values of k, but it is clear from Eq. 17 that only the pure bending mode with $k = 1$ and $q = \pi/L$ will make a significant contribution to the measurement.

To calculate the relaxation time for this mode, we calculate the elastic restoring force due to curvature, equate it to the radial component of the viscous stress tensor of the creeping fluid, and require that the radial velocity of the fluid at the cylindrical surface be equal to $\partial s/\partial t$.

The radial restoring force per unit membrane area is given by the negative of the functional derivative of the free energy in Eq. 15:

$$\bar{F}_{\text{norm}} = -K_C(\nabla^4 s + 2\nabla^2 s/a^2 + s/a^4)\,\tilde{\rho} \tag{18}$$

where $\tilde{\rho}$ is the unit vector in the radial direction. For the bending mode of interest,

$$\bar{F}_{\text{norm}} = -K_C\left(\frac{\pi}{L}\right)^4 S_{11}(t)\cos\psi\cos\frac{\pi z}{L}\,\tilde{\rho}. \tag{19}$$

Taylor (34) has solved the creeping motion equations for the fluid outside of an undulating cylinder of finite length. The problem he considers is the same as ours except that he employs slightly different boundary conditions. Instead of describing the $k = 1$ mode as a pure radial displacement (which preserves the circular cross section to first order), he uses radial and tangential displacements such that the net displacement of every point on a circular cross section is identical. The radial component of his displacement is identical to ours, and, because a displacement and restoring force along the ψ direction have, to first order, no influence on our problem, our calculation can be modified to use his results.

If the displacement in the radial direction is $S_{11}\cos\psi\cos(\pi z/L)$, to have the cylinder move as shown in Fig. 4, the displacement in the ψ direction must be $-S_{11}\sin\psi\cos(\pi z/L)$. If the wavelength, $2L$, is long compared with the radius of the cylinder, then, by symmetry, the restoring force at $\psi = 0$ must be the same as the restoring force at $\psi = \pi/2$ because both membrane elements move identically. The tangential restoring force of the membrane is then

$$\bar{F}_{\text{tan}} = K_C\left(\frac{\pi}{L}\right)^4 S_{11}(t)\sin\psi\cos\frac{\pi z}{L}\,\tilde{\Psi}, \tag{20}$$

where $\tilde{\Psi}$ is the unit normal vector in the circumferential direction.

In this limit, when the circular cross section moves with velocity V, Taylor's expressions for the normal and tangential components of the viscous force per unit area at $\rho = a$ are (34)

$$\bar{\sigma}_{\text{norm}} = \frac{2\eta}{a}\frac{1}{\ln(L/a) - 0.53}\,V\cos\psi\cos\frac{\pi z}{L}\,\tilde{\rho}, \tag{21a}$$

and

$$\bar{\sigma}_{\text{tan}} = -\frac{2\eta}{a}\frac{1}{\ln(L/a) - 0.53}\,V\sin\psi\cos\frac{\pi z}{L}\,\tilde{\Psi}, \tag{21b}$$

respectively.

At the cylinder surface, $V = \partial s/\partial t = -1/\tau_{11})\,S_{11}e^{-t/\tau_{11}}$. Upon setting Eq. 21a equal to Eq. 19 or Eq. 21b equal to Eq. 20, we find $S_{11}(t) = S_{11}e^{-t/\tau_{11}}$, where

$$\tau_{11} = \frac{2\eta}{K_C}\left(\frac{L}{\pi}\right)^3\frac{1}{\pi[\ln(L/a) - 0.53]}\,(L/a). \tag{22a}$$

The correlation function measured is, then, of $u(t) = s(0,0,t) - s(0,L/2,t)$. From Eqs. 14, 17, and 22, this is, with $q = \pi/L$,

$$\frac{\langle u(\tau)u(0)\rangle}{L^2} = \frac{2k_bT}{K_C\pi^5}\,(L/a)\,e^{-\tau/\tau_{11}} \tag{22b}$$

where τ_{11} is given by Eq. 22a.

This is identical to the expression in Eq. 13 except that the relaxation times differ by a factor of 2. This is not surprising because in the derivation of Eq. 13 it is assumed that, because $u \geq a$, the Stokeslet sources are linear over a distance 0.18 L. If $u << a$, the Stokeslet sources are linear over a longer distance, so $(cb)^{1/2} > 0.18L$ in Eq. 11, thus reducing the drag per unit length and also the relaxation time (Eq. 13).

Experimentally, the region of interest is $\langle u^2\rangle^{1/2} \sim a$. Because this range is intermediate to the two limiting theories that yield identical theoretical expressions for the measured correlation function except for a factor of 2 in the expressions for τ_C, the numerical coefficient is simply taken as the average of the limiting values. That is,

$$\frac{\langle u(\tau)u(0)\rangle}{L^2} = \frac{2k_bT}{K_C\pi^5}\frac{L}{a}\,e^{-\tau/\tau_C}, \tag{23a}$$

where

$$\tau_C \simeq \frac{3\eta}{K_C}\left[\frac{L}{\pi}\right]^3\frac{1}{\pi[\ln(L/a) - 0.53]}\frac{L}{a}. \tag{23b}$$

Wall Effects

The previous calculations for the viscous drag of the fluid assumes that the cylinder is moving in an infinitely large container. A nearby wall modifies the velocity field because all velocities must vanish at the wall. In our experiments, the vesicles are in glass containers. The average distance to the wall parallel to the plane in which the cylinder fluctuates is $\sim L$. In the absence of a wall, the velocity field around a straight circular cylinder moving perpendicular to its axis does not decay as fast as $1/\rho$ until the linear array of Stokeslet sources look like a point source, i.e., when $\rho \simeq L$ (27–29). The effect of a wall is an increase of the viscous drag on the cylinder (27,29) and therefore an increase in the relaxation time.

For a tube undulating in a plane parallel to a distant wall with $u \geq a$ the array of Stokeslet sources is linear for a distance $\sim 0.18L$; so for distances greater than this from the cylinder, the velocity field is expected to decay like $0.18\,L/\rho$ (29). When $u << a$, in the absence of a wall, the velocity field decays like a/ρ at $\rho \sim 0.3L$, and it decays faster than $e^{-\pi\rho/L}$ for $\rho \geq 0.6\,L$ (34). In both cases, in the absence of a wall, the velocity field will have significantly decayed at distances $\sim L$. Therefore, we assume that a wall at a distance L from the plane of the fluctuating cylinder has no measurable effect on the relaxation time.

MATERIALS AND METHODS

Vesicles were formed from a stock solution containing 50 mg egg phosphotidylcholine (Applied Science Div., Milton Roy Co., Laboratory Group, State College, PA) in 5 ml 2:1 vol/vol chloroform/methanol and 5×10^{-4} mol fraction 3,3'-dihexadecylindocarbocyanine iodide (diI) (35), a fluorescent lipid analogue (a generous gift of Dr. Alan S. Waggoner, Carnegie Mellon Univ.). Sometimes the lipid and dye were desalted by adding some water, shaking gently, and decanting the water. After repeating the procedure two times, the solvent was evaporated and fresh solvent added. A 10-μl drop of this solution was placed on a glass slide that had been cleaned in hot chromic-sulfuric acid. The slide was held at 40°C

until the solvent had evaporated. A 100-μl drop of deionized, doubly distilled water was gently placed on the lipid deposit and the specimen was left in a water saturated atmosphere for ~1 h. A good supply of thin-layered vesicles was obtained by sampling the solution with a 50-μm path length microslide (Vitro Dynamics, Inc., Rockaway, NJ) near the opaque lipid deposit. The ends of the microslide were then sealed onto a glass slide with Torr Seal (Varian, Palo Alta, Ca.) to prevent evaporation. For a better yield of the larger vesicles, the contents of the microslide was allowed to swell overnight. This method produced several thin-walled isolated long tubes per microslide plus many other types of vesicles that were usually attached to each other.

Experimental Procedure

If the outside walls of the microslide are extremely clean, the vesicles can be observed using phase contrast microscopy (36, 37), but the most convenient way we have found to observe single bilayer vesicles is with fluorescence microscopy. A 100-W high-pressure mercury lamp attached to a Zeiss Universal microscope (Carl Zeiss, Inc., Thornwood, NY) was used to excite the fluorescence of the dye molecules in the vesicle walls. An intensity of ~0.1 $\mu W/\mu m^2$ fell in the center of the illuminated field of a 40x microscope objective. To provide applicable data on deformations for the two-dimensional theories, only cylindrical vesicles that were in focus over their entire length during the observations were analyzed. The depth of field of the microscope objective was ~2 μm. The time course of the fluctuations of the chosen cylindrical vesicle was observed with a DAGE-MTI (Michigan City, IN) 650 SIT television camera that was mounted on the microscope. The television signal was recorded on video tape using a reel-to-reel video tape recorder (Panasonic Co., Div. Matsushita Electric Corp. of America, Secaucus, NJ, model NV-8030) (Fig. 5). For analysis, the timing in the signal from the video tape recorder played at real time speed was adjusted by a time-base corrector (Microtime, Inc., Bloomfield, CT, model 2020) so that the video signal could be read into the 6-bit digitizer of an Image Processing System (Grinnell Systems, San Jose, CA) and stored in the hard disk memory (Kennedy, Monrovia, CA, Model S303) of a DEC-LSI 11/20 computer system (Digital Equipment Corp., Maynard, MA) (Fig. 5). The computer had enough memory to store 175 (quarter) frames.

Each frame was analyzed by recalling it into the Grinnell memory bank, displaying it on a television monitor, and manually positioning a cursor at each end and at the center of the cylinder's axis. The computer read the location of the cursor and calculated $L(t)$ and $u(t)$ for that frame (Fig. 1). For consistency, the length of the cylinder was defined as shown in Fig. 1. The diameter of the cylinder was measured in the first frame of the series. If N is the total number of consecutive video frames analyzed and the frames are spaced Δt seconds apart, the correlation function is calculated from the formula

$$G(j\Delta t) = \sum_{i=1}^{N-j} \frac{u(i\Delta t)u(i\Delta t + j\Delta t)}{N - j}. \qquad (24)$$

The number of bilayers in the vesicle's wall is measured by obtaining a density tracing of the fluorescence intensity vs. distance from the cylinder axis along a line that is normal to the cylinder axis (Fig. 1 *b*). The maximum brightness in the tracing across a cylinder of a given diameter is proportional to the number of bilayers in the wall. To calibrate the number of bilayers, density tracings of ~10 thin-walled cylinders were taken each day for each vesicle preparation. Those vesicles with the lowest level fluorescence intensity were assumed to be single bilayers. The fluorescence intensity of thin multibilayer vesicles was observed to be approximately an integer multiple of that of single bilayer vesicles with the same diameter.

We are theoretically limited to a choice of vesicles with an L/a ratio of less than ~20 (assuming $K_C \sim 10^{-12}$ ergs) because the theoretical approximations require $(\langle u^2 \rangle / L^2)^{1/2} << 1$ (Eqs. 9, 17). To be considered a cylinder, L/a must be greater than ~10. The total time of observation, and hence the maximum measurable correlation time was experimentally limited by the slow photobleaching of the dye in the membranes during the observation. If all 175 frames were to be collected, the longest time possible between frames was ~7 s, because the dye photobleaches in ~20 min. Because the computer could not store the frames any faster than every 0.9 s, the minimum time of observation was also limited. Thus, the measurable range of values for the correlation time, τ_C, is $5\text{ s} \leqq \tau_C \leqq 50\text{ s}$. Because L/a is theoretically fixed (to within a factor of 2) and $\tau_C \sim L^3(L/a)$ (Eqs. 13, 22), we were limited to measuring tubes of length $14\ \mu\text{m} \leqq L \leqq 32\ \mu\text{m}$. The lower limit on L was very hard to reach because the amplitude of the fluctuations was quite small (Eqs. 13, 23).

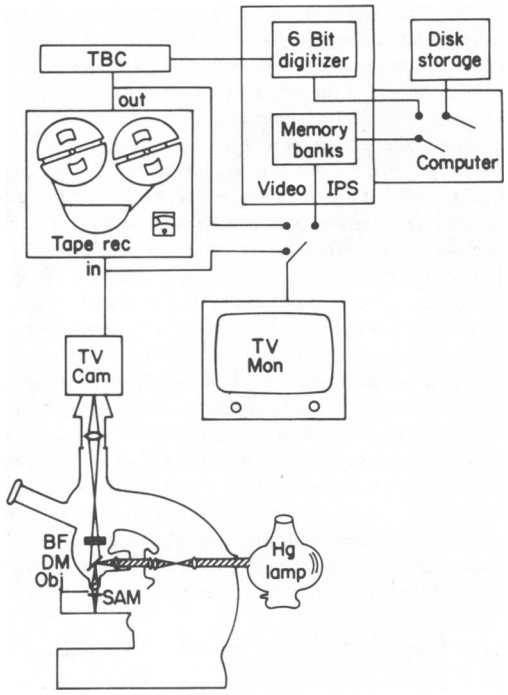

FIGURE 5 Schematic diagram of the experimental apparatus. The light from the mercury (Hg) lamp enters the vertical illuminator of a Zeiss Universal microscope (Carl Zeiss, Inc.) and is reflected downward by the dichroic mirror (DM) through the objective (OBJ) and onto the fluorescent sample (SAM) in the object plane of the microscope. Fluorescence is collected by the objective; it passes upward through the dichroic mirror and barrier filter (BF), which absorbs the mercury light, and is imaged at the focal plane of the microscope. A lens refocuses the fluorescent image onto the television camera (TV Cam). The image is recorded on video tape by the tape recorder (Tape rec), and simultaneously watched on the television monitor (TV Mon). The data to be analyzed are stored in the computer by passing the signal from the video tape recorder through a time base corrector (TBC), which corrects the timing in the signal so that the signal can be read into the image processing system (VIDEO IPS). The signal is digitized by the 6-bit digitizer in the IPS, and the computer stores the image of the vesicle every Δt seconds in the hard disk storage. To analyze an image, the computer recalls the image into one of the memory banks of the IPS. The image in the memory bank is displayed in the television monitor, and is analyzed as described in the text.

RESULTS

A typical set of data is shown in Fig. 6 *a*. The bars represent the error in locating the position in the digitized television image of the axis of the cylinder at the center and end points of the cylinder (Fig. 1). The correlation function, $G(j\Delta t)$, calculated from the data is shown in Fig. 6 *b*.

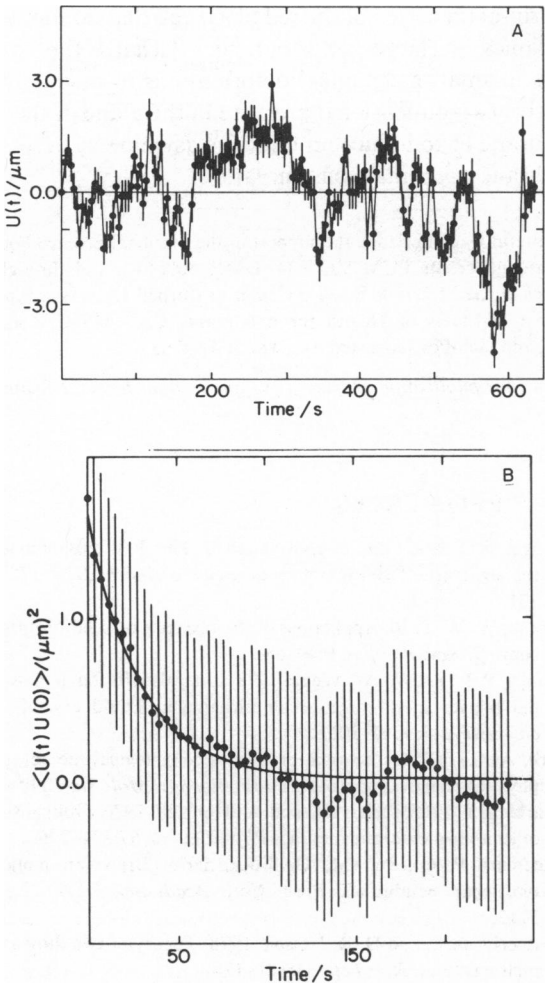

FIGURE 6 The data and calculated correlation function for a cylindrical vesicle whose length is 28 μm and whose length-to-diameter ratio is 7.8. (*A*) $u(t)$ vs. t. (*B*) The calculated correlation function.

The error bars, $(\sigma^2)^{1/2}$, for $G(j\Delta t)$ (Eq. 24) are determined from the formula

$$\sigma^2(j\Delta t) = \frac{\frac{2N\Delta t}{\tau_C} - 1 + 2e^{-N\Delta t/\tau_C} + \left[\left(\frac{2j\Delta t}{\tau_C} + 1\right)\left(\frac{2N\Delta t}{\tau_C} - 1\right) - 2\left(\frac{j\Delta t}{\tau_C}\right)^2\right]}{2(N\Delta t/\tau_C)^2} \cdot e^{-2j\Delta t/\tau_C} \quad (25)$$

where τ_C is the correlation time (38). Because $G(j\Delta t)$ is a random variable, the error in its measurement is expected to be $\sim N^{-1/2}$; however, adjacent points in the sum used to calculate $G(j\Delta t)$ (Eq. 24) are correlated over a time τ_C. Therefore, the total number of independent time intervals in Eq. 24 is $N\Delta t/\tau_C$ not N, so the error should be $\sim(N\Delta t/\tau_C)^{-1/2}$, as Eq. 25 implies. Because the computer limits N to 175 points, or ~17 correlation times, the curvature elastic modulus is measurable to within a factor of 2.

A weighted, linearized, least-squares routine (39) is used to fit the correlation function to an exponential decay, treating the amplitude and time as independent variables. The fit is also shown in Fig. 6 *b*.

The results for several cylindrical vesicles with the most complete measurements are shown in Table I. The estimated errors for K_C, determined independently from the amplitude and the time, correspond to one standard deviation. (The probability that the parameter falls within the indicated range of error is ~68% [39].) All additional data with larger uncertainties were consistent with these results. The vesicles were usually in the center of the 50-μm path length microslides so the effect of the wall on the viscous damping was neglected. We found $\langle u^2\rangle^{1/2} \simeq a$. The assumption of small fluctuations ($L >> u$) is justified. Separate values are given for the curvature elastic modulus deduced from the measured relaxation times (Eq. 23) and the amplitude. Using just the mean values in Table I, the average and standard deviations for K_C from the four cylinders are

$$K_C(\text{time}) = 1.7 \pm 0.7 \times 10^{-12}\ \text{ergs}$$
$$K_C(\text{amp}) = 1.2 \pm 0.5 \times 10^{-12}\ \text{ergs}. \quad (26)$$

It is concluded from all of the measurements that $K_C \sim 1$–2×10^{-12} ergs.

Servuss et al. (12) found the curvature elastic modulus of similar long cylindrical tubes by measuring the mean-square value of the difference in slope between the two tube ends. If our normal mode expansion (Eq. 6) for the shape of the cylinder was used rather than the one in reference 12, then our expression for the curvature elastic modulus was 0.81 times the expression found in reference 12. This put their value for K_C within our error. Values for K_C within our error were obtained whether the amplitude of the W was measured directly, as above, or whether we repeat the Servuss et al. experiment.

CONCLUSIONS

We have used a video imaging technique to measure the time correlation function of the fundamental bending mode of long cylindrical phospholipid vesicles. From these experiments, we found that the values of the curvature elastic modulus deduced separately from the correlation

TABLE I
RESULTS ON CYLINDRICAL VESICLES

L	L/a	$\langle u^2\rangle^{1/2}/a$	No. of layers	K_C (10^{-12} ergs)	
				Amplitude	Time
μm					
31.0	14.8	0.87	1	1.1 ± 0.1	2.7 ± 0.5
29.9	18.1	1.2	1	1.1 ± 0.3	0.94 ± 0.4
24.4	13.6	1.0	1	0.7 ± 0.1	1.4 ± 0.3
27.9	15.7	0.7	1	1.9 ± 0.5	1.7 ± 0.6

amplitude and time are in agreement, and, therefore, either measurement is sufficient to determine the curvature modulus. We conclude that $K_C \sim 1\text{–}2 \times 10^{-12}$ ergs.

It would be interesting to use this method to deduce values for the temperature and composition dependence of the curvature modulus of phospholipid membranes in regimes of physiological interest. Because small-amplitude bending deformations (at constant area) of flaccid membranes should be dominated by the curvature modulus, a similiar analysis (Schneider et al., manuscript in preparation) should be applicable to describe some of the mechanics of eucaryotic cell membranes. Thus, several distinctive cell membrane properties may be modulated by the temperature and composition dependence of the curvature modulus or its asymmetry. Large-scale deformations and deformations of nonflaccid cells would involve other properties of the cell membrane, particularly the cytoskeleton, and other membrane properties such as its shear modulus and area stretching modulus (22, 23).

We have observed that the amplitude of the fluctuations of vesicles made from a pure phosphatidylcholine seemed to increase on cooling to the vicinity of the gel phase transition temperature. These larger-amplitude fluctuations accompanied, perhaps, with local fluctuations in membrane asymmetry (spontaneous curvature) may be responsible for the enhanced membrane fusion frequently reported for lipid vesicles near phase transitions.

The success of the theoretical mechanics we have used to describe the bending mode fluctuations is encouraging, but these theories do not apply to the peristaltic fluctuations of the long tubes, because they do not accomodate the predicted instability in their present form. We have observed stable peristaltic fluctuations in cylindrical vesicles. We believe that a more detailed theory, analogous to the one we have developed in Schneider et al. (in preparation) for quasi-spherical vesicles, that better approximates the actual shapes and that strictly conserves the area and volume of the vesicle during the fluctuations, would be able to describe the peristaltic fluctuations.

Jenkins (16) has used a curvature elastic theory to calculate the equilibrium shapes of axisymmetric vesicles as a function of their area and volume. In another manuscript, Schneider et al. (in preparation), we extend his work to describe the thermal fluctuations of a quasi-spherical vesicle. We find that the expression for the correlation time contains a contribution from the two-dimensional hydrostatic pressure in the plane of the membrane. We believe that a similar analysis applied to the experimental results of Brochard and Lennon (17) would show the effective curvature elastic modulus of the red blood cell to be close to that of our artificial vesicles. This conjecture is supported by recent work of Evans (40) who used nonlinear deformations of the red blood cell to determine a value for the curvature modulus. He found $K_C \sim 1.8 \times 10^{-12}$ ergs, in agreement with Eq. 26. This result seems surprising in view of the known membrane asymmetry and characteristic spectrin-actin cortex of the red blood cell that dominates its mechanics in large deformations. Perhaps this cortex serves in small mechanical deformations to modulate the effective two-dimensional pressure in the plane of the lipid membrane or to induce an effective asymmetry across the membrane or spontaneous curvature.

We gratefully acknowledge the support of the National Science Foundation through grants PCM 8007634, DMR 8006513, and through the facilities of the Materials Science Center at Cornell University, and the National Institutes of Health through grants CA 14454C, and GM 21661, and facilities supported by grant 5P41 27533.

Received for publication 14 June 1983 and in final form 22 September 1983.

REFERENCES

1. Singer, S. J., and G. L. Nicholson. 1972. The fluid mosaic model of the structure of cell membranes. *Science (Wash. DC).* 175:720–731.
2. Webb, W. W. 1976. Applictions of fluorescence correlation spectroscopy. *Q. Rev. Biophys.* 9:49–68.
3. Fahey, P. F., and W. W. Webb. 1978. Lateral diffusion in phospholipid bilayer membranes and multilamellar liquid crystals. *Biochemistry.* 17:3046–3053.
4. Lee, A. G. 1975. Functional properties of biological membranes: a physical-chemical approach. *Prog. Biophys. Mol. Biol.* 29:5–56.
5. Harbich, W., R. M. Servuss, and W. Helfrich. 1976. Optical studies of lecithin-membrane melting. *Phys. Lett. A.* 57:294–296.
6. Saffman, P. G., and M. Delbruck. 1975. Brownian motion in biological membranes. *Proc. Natl. Acad. Sci. USA.* 72:3111–3113.
7. Halperin, B. I., and D. R. Nelson. 1978. Theory of two-dimensional melting. *Phys. Rev. Lett.* 41:121–124.
8. Birgeneau, R. J., and J. D. Litster. 1978. Bond orientational order model for smectic B liquid crystals. *J. Phys. (Paris).* 39:L399–402.
9. Jenkins, J. T. 1977. The equations of mechanical equilibrium of a model membrane. *SIAM (Soc. Ind. Appl. Math.) J. Appl. Math.* 32:755–764.
10. Helfrich, W. 1973. Elastic properties of lipid bilayers: theory and possible experiments. *Z. Naturforsch. Sect. C. Biosci.* 28:693–703.
11. Deuling, H. J., and W. Helfrich. 1976. The curvature elasticity of fluid membranes: a catalogue of vesicle shapes. *J. Phys. (Paris).* 37:1335–1345.
12. Servuss, R. M., W. Harbich, and W. Helfrich. 1976. Measurement of the curvature-elastic modulus of egg lecithin bilayers. *Biochim. Biophys. Acta.* 436:900–903.
13. Kwok, R., and E. Evans. 1981. Thermoelasticity of large lecithin bilayer vesicles. *Biophys. J.* 35:637–652.
14. Waugh, R. E. 1982. Surface viscosity measurements from large bilayer vesicle tether formation. I. Analysis. *Biophys. J.* 38:19–27.
15. Waugh, R. E. 1982. Surface viscosity measurements from large bilayer vesicle tether formation. II. Experiments. *Biophys. J.* 38:29–37.
16. Jenkins, J. T. 1977. Static equilibrium configurations of a model red blood cell. *J. Math. Biol.* 4:149–169.
17. Brochard, F. and J. F. Lennon. 1975. Frequency spectrum of the flicker phenomenon in erythrocytes. *J. Phys. (Paris).* 36:1035–1047.
18. Blowers, R., E. M. Clarkson, and M. Maizels. 1951. Flicker phenomenon in human erythrocytes. *J. Physiol. (Lond.).* 113:228–239.

19. Parpart, A. K., and J. F. Hoffman. 1956. Flicker in erythrocytes. Vibratory movements in the cytoplasm? *J. Cell Comp. Physiol.* 47:295–303.
20. Lux, S. E. 1979. Dissecting the red cell membrane skeleton *Nature (Lond.).* 281:426–429.
21. Sheetz, M. P., M. Schindler, and D. E. Koppel. 1980. Lateral mobility of integral membrane proteins is increased in spherocytic erythrocytes. *Nature (Lond.).* 285:510–512.
22. Evans, E. A., and R. M. Hochmuth. 1978. Mechanochemical properties of membranes. *Curr. Top. Membr. Transp.* 10:1–64.
23. Evans, E. A., and R. Skalak. 1979. Mechanics and Thermodynamics of Biomembranes. I. *Crit. Rev. Bioeng.* 3:181–418.
24. Eisenhart, L. 1947. An Introduction to Differential Geometry. Princeton University Press, Princeton, NJ. 1–250.
25. deGennes, P. G., and M. Papoular. 1969. Vibrations de basse frequence dans certaines structures biologiques. *In* Polarisation Matière et Rayonnement. Presses universitaires de France, Paris. Société Française de Physique, editor. 243–258.
26. Landau, L. D., and E. M. Lifshitz. 1969. Statistical Physics Pergamon Press, Oxford. 370–374.
27. Happel, J., and H. Brenner 1973. Low Reynolds Number Hydrodynamics. Noordhoff International Publishing, Alphen aan den Rijn, The Netherlands. 71–78.
28. Lamb, H. 1932. Hydrodynamics. Cambridge University Press, Cambridge, England. 562–691.
29. Lighthill, J. 1975. Mathematical Biofluiddynamics. The Society for Industrial and Applied Mathematics, Philadelphia. 43–53, 141–144.
30. Boys, C. V. 1959. Soap Bubbles. Dover Publications Inc., Mineola, NY. 62–71.
31. Nageotte, J. 1936. Morphologie des Gels Lipoides. Hermann and Cie. Paris. Vol. IV. Plate V.
32. Boroske, E., M. Elwenspoek, and W. Helfrich. 1981. Osmotic shrinkage of giant egg-lecithin vesicles. *Biophys. J.* 34:95–109.
33. Coakley, W. T., A. J. Bater, and J. O. T. Deeley. 1978. Vesicle production on heated and stressed erythrocytes. *Biochim. Biophys. Acta.* 512:318–330.
34. Taylor, G. 1952. The action of waving cylindrical tails in propelling microscopic organisms. *Proc. Royal Soc. A.* 211:225–239.
35. Sims, P. J., A. S. Waggoner, C.-H. Wang, and J. F. Hoffman. 1974. Studies on the mechanism by which cyanine dyes measure membrane potential in the red blood cells and phosphatidylcholine vesicles. *Biochemistry.*13:3315–3330.
36. Servuss, R. M., and E. Boroske. 1979. Lamellarity of artificial phospholipid-membranes determined by photometric phase-contrast microscopy. *Phys. Lett.* A. 69:468–470.
37. Servuss, R. M., and E. Boroske. 1980. Dependence of the optical contrast of vesicle walls on lamellarity and curvature. *Chem. Phys. Lipids.* 27:57–69.
38. Bendat, J. S. 1977. Principles and Applications of Random Noise Theory. R. E. Krieger Publishing Co. Inc., Melbourne, FL. 266–271.
39. Bevington, P. R. 1969. Data Reduction and Error Analysis for the Physical Sciences. McGraw-Hill, Inc., New York. 204–246.
40. Evans, E. A. 1983. Bending elastic modulus of red blood cell membrane derived from buckling instability in micropipet aspiration tests. *Biophys. J.* 43:27–30.